

## UNSTABLE DISK GALAXIES. II. THE ORIGIN OF GROWING AND STATIONARY MODES

MIR ABBAS JALALI

Sharif University of Technology, Azadi Avenue, Tehran, Iran; mjalali@sharif.edu  
 Institute for Advanced Study, Einstein Drive, Princeton, NJ 08540  
*The Astrophysical Journal, In Press*

### ABSTRACT

I decompose the unstable growing modes of stellar disks to their Fourier components and present the physical mechanism of instabilities in the context of resonances. When the equilibrium distribution function is a non-uniform function of the orbital angular momentum, the capture of stars into the corotation resonance imbalances the disk angular momentum and triggers growing bar and spiral modes. The stellar disk can then recover its angular momentum balance through the response of non-resonant stars. I carry out a complete analysis of orbital structure corresponding to each Fourier component in the radial angle, and present a mathematical condition for the occurrence of van Kampen modes, which constitute a continuous family. I discuss on the discreteness and allowable pattern speeds of unstable modes and argue that the mode growth is saturated due to the resonance overlapping mechanism. An individually growing mode can also be suppressed if the corotation and inner Lindblad resonances coexist and compete to capture a group of stars. Based on this mechanism, I show that self-consistent scale-free disks with a sufficient distribution of non-circular orbits should be stable under perturbations of angular wavenumber  $m > 1$ . I also derive a criterion for the stability of stellar disks against non-axisymmetric excitations.

*Subject headings:* stellar dynamics, instabilities, methods: analytical, galaxies: kinematics and dynamics, galaxies: spiral, galaxies: structure

### 1. INTRODUCTION

Both  $N$ -body simulations (Hohl 1971) and analytical methods (Kalnajs 1978; Jalali & Hunter 2005, hereafter JH) show that global instabilities can generate barred structures in galactic disks. Apart from the bar mode, which is an isolated event in frequency space, global spiral modes seen in the eigenspectra of cored stellar disks (Jalali 2007, hereafter Paper I) constitute a discrete family that bifurcates from stationary van Kampen (1955) modes. But not all spiral structures are global modes as disturbances induced by close neighbors (Byrd & Howard 1992) and density inhomogeneities (Toomre 1990) may also create the spiral patterns of the observed galaxies.

A mode of a stellar disk is a mathematical entity that comes out of an eigenvalue problem. However, its physical origin in isolated systems has not yet been understood clearly. Lynden-Bell & Kalnajs (1972, hereafter LBK) attempted to explain a mode through the transport of angular momentum between different parts of the disk. They suggested that the inner Lindblad resonance (ILR) releases the angular momentum of central regions and the spiral structure transports it to the outer parts through the corotation (CR) and outer Lindblad resonances (OLR). This mechanism is favored by some galactic dynamicists (Athanasoula 2003), but it is seriously challenged by Toomre's (1981) theory that says that feedback through the galactic center is a critical ingredient for growing modes. In Toomre's theory, on the other hand, the modeling of feedback as the reflection of a leading spiral wave at the galactic center and its emergence as a trailing one, is a simple description of a very complicated dynamics that governs the motions of stars. Unresolved issues concerning the evolution of unstable modes include the following: (i) The swing amplification

theory is not capable of predicting the fate of a growing mode against other stationary and unstable modes that coexist in the eigenspectrum of a given model. (ii) How does the bar mode saturate? (e.g., Khoperskov et al. 2007). (iii) Why does the nonlinear bar terminate almost at the corotation radius? (Sellwood 1981) (iv) We should also understand the origin of different species in an eigenspectrum and interpret their continuous or discrete nature, and the distribution of their pattern speeds and growth rates.

Stellar orbits in a galactic disk begin to evolve once the surface density deviates from its equilibrium state,  $\Sigma_0(\mathbf{x})$ , and develops a time-varying mean-field potential  $V_1(\mathbf{x}, t)$ . Here  $\mathbf{x}$  denotes the position vector of stars at the time  $t$ . In the linear regime, we are usually interested in density waves that grow/decay according to the exponential law  $e^{st}$  and rotate with the fixed pattern speed  $\Omega_p$ . For a wave of  $m$ -fold symmetry, the perturbed potential becomes

$$V_1 = \epsilon e^{st} \tilde{V}(\mathbf{x}, m\Omega_p t). \quad (1)$$

Since we are dealing with infinitesimal perturbations, I have introduced the small parameter  $\epsilon$  so that  $\epsilon e^{st} \ll 1$ . From (1) one arrives at the equations of motion

$$\dot{\mathbf{x}} = \mathbf{v}, \quad \dot{\mathbf{v}} = -\frac{\partial V_0}{\partial \mathbf{x}} - \epsilon e^{st} \frac{\partial \tilde{V}}{\partial \mathbf{x}}, \quad (2)$$

where  $V_0(\mathbf{x})$  is the equilibrium potential field generated by galactic stars and a possible dark matter halo. In writing equation (2), I have assumed that the motion of stars is restricted to the disk plane. When the equilibrium state is axisymmetric and the dark component is spherical,  $V_0$  becomes a function of radial distance to the galactic center and the unperturbed equations (with  $\epsilon = 0$ ) are integrable. In such a circumstance, the phase

space is filled by rosette orbits denoted by  $[\mathbf{x}_0(t), \mathbf{v}_0(t)]$ . The growth of perturbations, whatever the magnitude of  $\epsilon e^{st} \ll 1$  may be, deforms stellar orbits. Orbital deformations are measured by  $\tilde{\mathbf{x}} = \mathbf{x} - \mathbf{x}_0$  and  $\tilde{\mathbf{v}} = \mathbf{v} - \mathbf{v}_0$ , which can be used in (2) to obtain

$$\frac{d\tilde{\mathbf{x}}}{dt} = \tilde{\mathbf{v}}, \quad \frac{d\tilde{\mathbf{v}}}{dt} = - \left[ \frac{\partial^2 V_0}{\partial \mathbf{x}^2} \right]_{\mathbf{x}_0} \cdot \tilde{\mathbf{x}} - \epsilon e^{st} \left[ \frac{\partial \tilde{V}}{\partial \mathbf{x}} \right]_{\mathbf{x}_0}. \quad (3)$$

Although a proper equilibrium distribution function  $f_0(\mathbf{x}, \mathbf{v})$  can self-consistently reproduce  $\Sigma_0(\mathbf{x})$  using rosette orbits, the perturbed density  $\Sigma_1(\mathbf{x}, t)$  (corresponding to  $V_1$ ) cannot be supported by rosette orbits alone and orbital deformations are necessary for the self-consistency of density waves. According to equations (2) and (3), orbital deformations of  $\mathcal{O}(\epsilon e^{st})$  are sufficient to support the growth of density/potential perturbations up to the same order of magnitude of such deformations over a time scale of  $1/\mathcal{O}(\epsilon e^{st})$ . As the time is elapsed, the amplitude of perturbations increases exponentially and the solution of the linearized collisionless Boltzmann equation (CBE) fails when  $\epsilon e^{st} \sim 1$ . During my mode calculations, I realized that the orbital axes of certain stars librate in a coordinate frame that rotates with the density pattern. This *resonant capture* initially seemed to be a higher-order nonlinear effect but further experiments showed that the resonant gap is constrained by the magnitude of density perturbations. The complex behavior of stars for infinitesimally small yet non-zero  $\epsilon e^{st} \ll 1$ , and the role of resonant stars in the generation of discrete galactic modes, are investigated in this paper.

I use the results of Paper I and introduce a new dynamical mechanism that sparks unstable modes and governs the singular oscillations of van Kampen (1955) modes. Resolving the origin of instabilities and amplitude saturation precede my nonlinear calculations, which were made feasible in Paper I by the Petrov-Galerkin method and reducing the CBE to a system of nonlinear ordinary differential equations. Those reduced equations, however, are valid only when orbits are regular and averaging over angle variables is allowed. As unstable modes grow, chaotic orbits come into existence and the weighted residual form of the CBE must be modified to handle them. I quote some of the results of such modifications in this paper when I discuss the issue of mode saturation. In Paper III, I will give a full account of the mathematical and numerical modeling of stochastic layers, and will analyze modal interactions after their saturation phase.

For the cored exponential disk embedded in the field of the cored logarithmic potential, I describe the decomposed Fourier components of unstable bar and spiral modes in §3 and highlight the existence of a phase shift between different components. In §4, I derive a condition for the corotation of the orbital axes of an ensemble of stars and explain the role of such a synchronous motion in pattern formation. I dedicate §5 to exploring the orbital structure of a perturbed stellar disk and identify a resonance mechanism that can generate both stationary and growing modes. I reveal the mechanism of angular momentum transfer between Fourier components and derive analytical expressions for the growth of resonance zone. I address the origin of instabilities in §6, present a saturation mechanism for unstable modes in §7, and

discuss about the global stability of soft-centered and scale-free disks. I explain the restrictions of LBK's mode mechanism in §8 and end up the paper with concluding remarks.

## 2. THE MODEL

The calculations of the present study are carried out for the cored exponential disks of JH whose eigenfrequency spectra and mode shapes have been completely explored in Paper I. The model has a dark matter halo and the motion of stars in the equilibrium state is governed by the cored logarithmic potential

$$V_0(R) = v_0^2 \ln \sqrt{1 + R^2/R_C^2}, \quad (4)$$

which is the resultant gravitational potential of luminous and dark components. Throughout the paper, all length and velocity variables are normalized, respectively, to the core radius of the potential ( $R_C$ ) and the asymptotic velocity of stars on circular orbits ( $v_0$ ) by setting  $R_C = v_0 = 1$ . To describe the physical quantities in the configuration space, I will use the usual polar coordinates  $(R, \phi)$  and their Cartesian counterparts  $(x, y)$  where  $R$  is the radial distance from the galactic center and  $\phi$  is the azimuthal angle. The specific model that I adopt here is a relatively cold, near-maximal disk with no dark matter concentration in the region with rising rotation curve. The model parameters are set to  $(N, \lambda, \alpha) = (6, 1, 0.42)$  where  $N$  is an integer exponent that controls the proportion of circular orbits and the disk temperature. Larger values of  $N$  give rise to colder disks. For  $N = 6$ , the parameter  $Q$  of Toomre (1964) is marginally larger than 1. The parameter  $\lambda$  is defined as the ratio  $R_C/R_D$  with  $R_D$  being the core radius of the equilibrium density.  $\alpha$  is a factor that controls the total mass of the stellar component. The chosen model with  $\alpha = 0.42$  is near-maximal within a radius of  $\approx 2.5R_C$  and dominated by dark matter beyond it. The calculations of Paper I revealed the eigenspectrum of this model that includes a compact bar mode B1 and a sequence of spiral modes S1,  $\dots$ , S6. I select modes B1 and S2 as my case studies of sections 3 through 5. The reason for choosing mode S2 is its extensive and prominent spiral structure and modest growth rate. In section 7, I will also display some results for modes S1, S3 and S6.

## 3. DECOMPOSITION OF UNSTABLE MODES

One of the advantages of the method developed in Paper I is that the density function of a mode can be readily decomposed to its constituent Fourier components in angle-action space. The phase shifts between density components determine the magnitude and direction of the torque that is exerted on each component. So we can probe the transfer of angular momentum and identify the direction of its flow once a global mode develops.

The perturbed distribution and Hamiltonian functions of an unstable mode can be expanded as (Paper I)

$$f_1(\Theta, \mathbf{J}, t) = \text{Re} \sum_{m, l = -\infty}^{\infty} \sum_{j=0}^{\infty} \epsilon d_j^{ml}(t) \Phi_j^{ml}(\mathbf{J}) e^{i(m\theta_\phi + l\theta_R)}, \quad (5)$$

$$\mathcal{H}_1(\Theta, \mathbf{J}, t) = \text{Re} \sum_{m, l = -\infty}^{\infty} \sum_{j=0}^{\infty} \epsilon b_j^{ml}(t) \Psi_j^{ml}(\mathbf{J}) e^{i(m\theta_\phi + l\theta_R)}, \quad (6)$$

where  $\Theta = (\theta_R, \theta_\phi)$  and  $\mathbf{J} = (J_R, J_\phi)$  are the angle and action variables, respectively. The angles are defined based on the radial and azimuthal frequencies

$$\boldsymbol{\Omega} = (\Omega_R, \Omega_\phi) = \left( \frac{\partial \mathcal{H}_0}{\partial J_R}, \frac{\partial \mathcal{H}_0}{\partial J_\phi} \right), \quad (7)$$

of stars on rosette orbits so that

$$\dot{\theta}_R = \Omega_R(\mathbf{J}), \quad \dot{\theta}_\phi = \Omega_\phi(\mathbf{J}). \quad (8)$$

A dot stands for the time derivative and  $\mathcal{H}_0(\mathbf{J})$  is the integrable Hamiltonian of the axisymmetric equilibrium state. For a normal mode the amplitude functions  $d_j^{ml}(t)$  and  $b_j^{ml}(t)$  depend on the time variable  $t$  through the simple exponential law  $\exp(-i\omega t)$  with  $\omega = m\Omega_p + \nu s$  and  $\nu = \sqrt{-1}$ . Here  $\Omega_p$  and  $s$  are the pattern speed and growth rate of an unstable mode of angular wavenumber  $m$ . On the other hand, the perturbed potential function  $V_1$  and its associated surface density  $\Sigma_1$  can be expanded in the configuration space as

$$V_1(R, \phi, t) = \text{Re} \sum_{m=-\infty}^{\infty} \sum_{j=0}^{\infty} \epsilon a_j^m(t) \psi_j^{|m|}(R) e^{im\phi}, \quad (9)$$

$$\Sigma_1(R, \phi, t) = \text{Re} \sum_{m=-\infty}^{\infty} \sum_{j=0}^{\infty} \epsilon a_j^m(t) \sigma_j^{|m|}(R) e^{im\phi}, \quad (10)$$

where  $\sigma_j^{|m|}(R)$  and  $\psi_j^{|m|}(R)$  are surface density and potential basis functions, respectively. They satisfy Poisson's integral and the bi-orthogonality condition

$$D_j(m) \delta_{j,j'} \delta_{m,m'} = 2\pi \int_0^\infty \psi_j^{|m|}(R) \sigma_{j'}^{|m'|}(R) R dR. \quad (11)$$

Here  $\delta_{m,m'}$  is the Kronecker delta and  $D_j(m)$  are some constants that depend on our special choice of basis functions. Noting  $V_1 \equiv \mathcal{H}_1$ , one can equate (6) and (9), multiply the identity by  $\exp[-i(l\theta_R + m\theta_\phi)]$  and integrate over the angle variables to obtain

$$\sum_{j=0}^{\infty} b_j^{ml}(t) \Psi_j^{ml}(\mathbf{J}) = \sum_{j=0}^{\infty} a_j^m(t) \tilde{\Psi}_j^{ml}(\mathbf{J}), \quad (12)$$

$$\tilde{\Psi}_j^{ml}(\mathbf{J}) = \frac{1}{\pi} \int_0^\pi \psi_j^{|m|}(R) \cos[l\theta_R + m(\theta_\phi - \phi)] d\theta_R. \quad (13)$$

Setting  $\Psi_j^{ml}(\mathbf{J}) = \tilde{\Psi}_j^{ml}(\mathbf{J})$  gives  $b_j^{ml}(t) = a_j^m(t)$ , which is a remarkable simplification. A relation between  $a_j^m(t)$  and  $d_j^{ml}(t)$  then follows from the weighted residual form of the fundamental equation

$$f_1(\Theta, \mathbf{J}, t) d\mathbf{J} d\Theta = \Sigma_1(R, \phi, t) R dR d\phi. \quad (14)$$

I obtain

$$a_j^m(t) = \frac{4\pi^2}{D_j(m)} \sum_{l=-\infty}^{\infty} \sum_{k=0}^{\infty} \Lambda_{jk}^{ml} d_k^{ml}(t), \quad (15)$$

$$\Lambda_{jk}^{ml} = \int \Psi_j^{ml}(\mathbf{J}) \Phi_k^{ml}(\mathbf{J}) d\mathbf{J}, \quad (16)$$

where

$$\Phi_k^{ml}(\mathbf{J}) = \frac{l(\partial f_0/\partial J_R) + m(\partial f_0/\partial J_\phi)}{l\Omega_R + m\Omega_\phi} \Psi_k^{ml}(\mathbf{J}). \quad (17)$$

Let  $\mathcal{L}$  be the total angular momentum of the disk, which must be conserved in an isolated galaxy. This means that the torque  $d\mathcal{L}/dt$  must vanish. Defining

$$a_j^m(t) = e^{-i\omega t} \bar{a}_j^m = e^{-i\omega t} (u_j^m + i v_j^m), \quad (18)$$

$$d_j^{ml}(t) = e^{-i\omega t} \bar{d}_j^{ml} = e^{-i\omega t} (U_j^{ml} + i V_j^{ml}), \quad (19)$$

one obtains

$$\frac{d\mathcal{L}}{dt} = 2m\pi^2 \epsilon^2 e^{2st} \sum_{l=-\infty}^{\infty} L_m(l) = 0, \quad (20)$$

$$L_m(l) = \sum_{j,k=0}^{\infty} \Lambda_{jk}^{ml} (v_j^m U_k^{ml} - u_j^m V_k^{ml}). \quad (21)$$

The constant vectors  $(U_k^{ml}, V_k^{ml})$  and  $(u_j^m, v_j^m)$  are obtained from the linear eigenvalue equations of Paper I and a subsequent use of equation (15). Equation (20) is analogous to equation (B6) in JH and  $L_m(l)$  shows the rate of angular momentum flow into/from the  $l$ th Fourier component (in the radial angle  $\theta_R$ ) whose corresponding density in the configuration space is

$$\Sigma_1^l = \epsilon e^{st} \text{Re} \sum_{j,k=0}^{\infty} \frac{4\pi^2}{D_j(m)} \Lambda_{jk}^{ml} \sigma_j^{|m|}(R) \bar{d}_k^{ml} e^{im(\phi - \Omega_p t)}. \quad (22)$$

The angular momentum conservation of the disk implies that some  $L_m(l)$  take negative and some other positive values with a total vanishing sum. This means that  $\Sigma_1^l$ , the pattern corresponding to  $L_m(l)$ , is subject to a positive torque from other components if  $L_m(l) > 0$ , and a negative torque otherwise.

Figure 1 shows the variation of  $L_2(l)$  versus  $l$  for modes B1 and S2. The results are in accordance with the bar charts of JH: components with  $l < 0$  lose angular momentum and those with  $l \geq 0$  gain it. As JH had already pointed out, a few components ensure the convergence of Fourier series in the  $\theta_R$ -direction. The superposition of the  $l \geq 0$  components of the perturbed density, defined as

$$\Sigma_1^{l+}(R, \phi, t) = \sum_{l=0}^{\infty} \Sigma_1^l(R, \phi, t), \quad (23)$$

will thus be a pattern that experiences a positive torque exerted by

$$\Sigma_1^{l-}(R, \phi, t) = \sum_{l=-\infty}^{-1} \Sigma_1^l(R, \phi, t). \quad (24)$$

In response, the reaction torque of  $\Sigma_1^{l+}$  will drain the angular momentum of  $\Sigma_1^{l-}$  so that  $\mathcal{L}$  is conserved. Figure 2 shows modes B1 and S2 and their components that emit and absorb angular momentum. It is seen that in both modes, the phase of  $\Sigma_1^{l+}$  lags that of  $\Sigma_1^{l-}$  by a magnitude of  $\approx 90^\circ$  and the positive parts of  $\Sigma_1^{l-}$  fill the regions of negative  $\Sigma_1^{l+}$ . Due to this phase shift, the angular momentum is transferred between  $l < 0$  and  $l \geq 0$  components and a counterclockwise torque is exerted on  $\Sigma_1^{l+}$ .

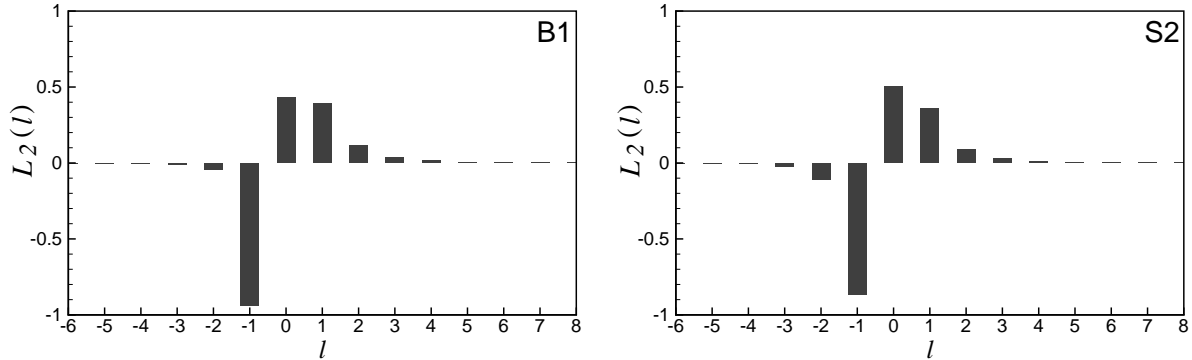


FIG. 1.— The angular momentum content of different Fourier components of modes B1 and S2. The sum  $\sum_{l=-\infty}^{+\infty} L_m(l)$  vanishes because the total angular momentum of the disk is conserved. The function  $L_m(l)$  is normalized so that the sum of positive components is unity.

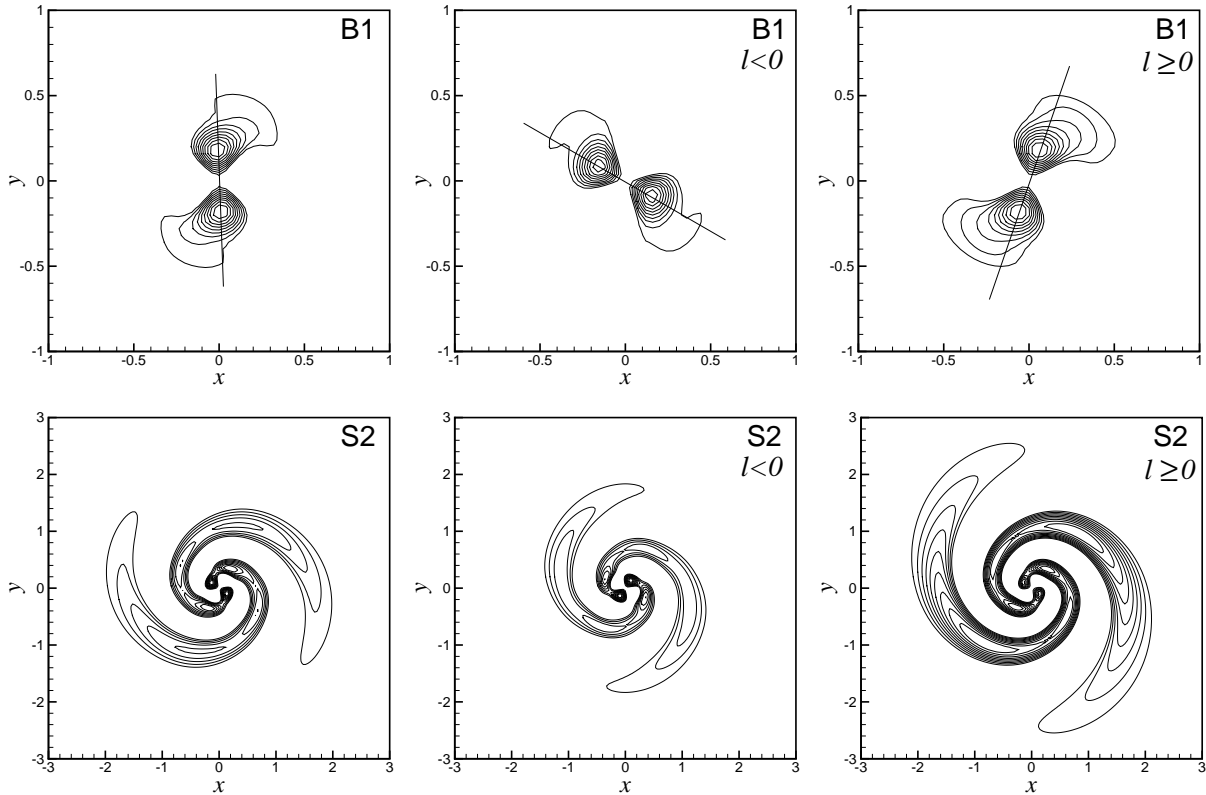


FIG. 2.— Modes B1 and S2 and their components that release and absorb angular momentum. Left panels show the mode shapes, which rotate counter-clockwise. The pattern speeds and growth rates of modes B1 and S2 are  $(\Omega_p, s) = (0.918, 1.160)$  and  $(\Omega_p, s) = (0.454, 0.216)$ , respectively. Middle and right panels demonstrate the  $\Sigma_1^{l-}$  and  $\Sigma_1^{l+}$  components, respectively. Solid lines in top panels highlight the orientations of the bar mode and its components. The prominent phase shift between  $\Sigma_1^{l-}$  and  $\Sigma_1^{l+}$  is responsible for the gravitational torque between them. The isocontours show the positive part of the density from 10% to 90% of the maximum with increments of 10%.

This phenomenon is more obvious in mode B1 that has a definite spatial orientation. The most important question relevant to the origin of instabilities arises now: Are the density components  $\Sigma_1(R, \phi, t)$  generated by stellar orbits at resonances? Analytical calculations of sections 4 and 5 provide the answer.

#### 4. SYNCHRONOUS PRECESSION OF THE ORBITAL AXES

The perturbed density  $\Sigma_1$  of a mode with the pattern speed  $\Omega_p$  must be supported by the slow motion of stars in a rotating coordinate frame of angular velocity  $\Omega_p$ . In other words, by sitting on a moving coordinate system

one must be able to identify a group of stars that are losing their angular velocity, and another group of the same kind but with different initial conditions, gaining it. A density peak is expected in the region that the angular velocity of the slow ensemble is minimum. Since the angular velocity of a star is minimum at its orbital apocenter, the precession rate of the orbital axes of participating stars in the pattern formation should be in resonance with the pattern speed. The above scenario is legitimate as long as pattern stars stay far from Lindblad resonances that can generate higher density regions due to the radial slowing of stars. My computations show

that all unstable modes fulfill this requirement and azimuthal slowing is the main origin of density perturbations (see §5).

The evolution of  $\phi(t)$  is crucial for understanding the slow dynamics in the configuration space, but we usually have the perturbed distribution and potential functions in the angle-action space. It is thus useful to find how  $\phi$  depends on  $(\Theta, \mathbf{J})$ . The simplest relation can be obtained by expanding  $\exp[i m(\phi - \theta_\phi)]$  in Fourier series of  $\theta_R$  as

$$e^{im(\phi - \theta_\phi)} = \sum_{l=-\infty}^{+\infty} \xi_{ml}(\mathbf{J}) e^{il\theta_R}, \quad (25)$$

where

$$\xi_{ml}(\mathbf{J}) = \frac{1}{2\pi} \oint \cos[l\theta_R + m(\theta_\phi - \phi)] d\theta_R. \quad (26)$$

The functions  $\xi_{ml}(\mathbf{J})$  are computed by integrating along rosette orbits (over a period of radial oscillation), and they vanish for circular orbits when  $l \neq 0$  and for radial orbits when  $m \neq -2l$ . Multiplying equation (25) by  $\exp[-im(\phi - \theta_\phi)]$  and integrating the identity over a period of  $\theta_R$  yields the following useful relation

$$\sum_{l=-\infty}^{+\infty} [\xi_{ml}(\mathbf{J})]^2 = 1. \quad (27)$$

Moreover, taking the partial derivative of (25) with respect to  $\theta_R$ , multiplying both sides of the resulting equation by  $\exp[-im(\phi - \theta_\phi)]$  followed by an integration over  $\theta_R$ , leads to (Scott Tremaine, private communication)

$$\sum_{l=-\infty}^{+\infty} l [\xi_{ml}(\mathbf{J})]^2 = 0. \quad (28)$$

I now multiply (25) by  $\exp(im\theta_\phi)$ , differentiate both sides of the resulting equation with respect to  $t$  and obtain

$$\begin{aligned} m\dot{\phi} = & -\text{Re} \sum_{l=-\infty}^{+\infty} i \left( \frac{\partial \xi_{ml}}{\partial J_R} \dot{J}_R + \frac{\partial \xi_{ml}}{\partial J_\phi} \dot{J}_\phi \right) e^{i(l\theta_R + m\theta_\phi - m\phi)} \\ & + \text{Re} \sum_{l=-\infty}^{+\infty} \xi_{ml} (l\dot{\theta}_R + m\dot{\theta}_\phi) e^{i(l\theta_R + m\theta_\phi - m\phi)}. \end{aligned} \quad (29)$$

The perturbed motions of stars are governed by Hamilton's equations

$$\dot{\Theta} = \Omega(\mathbf{J}) + \frac{\partial \mathcal{H}_1}{\partial \mathbf{J}}, \quad \dot{\mathbf{J}} = -\frac{\partial \mathcal{H}_1}{\partial \Theta}, \quad (30)$$

that can be used to rewrite (29) in the form

$$\begin{aligned} m\dot{\phi} = & \text{Re} \sum_{l=-\infty}^{+\infty} \xi_{ml} [l\Omega_R + m\Omega_\phi] e^{i(l\theta_R + m\theta_\phi - m\phi)} \\ & - \text{Re} \sum_{l=-\infty}^{+\infty} i e^{-im\phi} \left[ e^{i(l\theta_R + m\theta_\phi)} \xi_{ml}, \mathcal{H}_1 \right], \end{aligned} \quad (31)$$

where  $[\dots, \dots]$  denotes a Poisson bracket taken over the angle-action space. On substituting for the complex conjugate of  $\exp(im\phi)$  from (25) in (31) and noting that the

second term on the right hand side of (31) is of  $\mathcal{O}(\epsilon e^{st})$ , one finds

$$m\dot{\phi} = \text{Re} \sum_{l,k=-\infty}^{+\infty} \xi_{ml} \xi_{mk} [l\Omega_R + m\Omega_\phi] e^{i(l-k)\theta_R} + \mathcal{O}(\epsilon e^{st}), \quad (32)$$

which shows the functional dependence of  $\dot{\phi}$  on the actions and the radial angle.

Equation (32) can be written as

$$m\dot{\phi} = m\Omega_\phi(\mathbf{J}) + \eta(\mathbf{J}, \theta_R) + \mathcal{O}(\epsilon e^{st}), \quad (33)$$

where the constant part  $m\Omega_\phi$  is obtained by setting  $l = k$  in the double summation of (32) and subsequent application of relations (27) and (28).  $\eta(\mathbf{J}, \theta_R)$  is a periodic function of  $\theta_R$  that stands for all other terms of (32) with  $l \neq k$ .  $\Omega_\phi(\mathbf{J})$  is thus the precession rate of the orbital axis of stars whose energy and angular momentum correspond to the action vector  $\mathbf{J}$ . Those stars can contribute to a developing density peak when they linger at the apocenter of their orbits. Such a mass deposition will continue in a rotating frame of angular velocity  $\Omega_p$  and over the time scale  $1/\mathcal{O}(\epsilon e^{st})$  if the condition for synchronous precession

$$\left\langle \dot{\phi} \right\rangle_{\theta_R} - \Omega_p \approx \mathcal{O}(\epsilon e^{st}), \quad (34)$$

holds. By defining

$$\mu_m^l(\mathbf{J}) = l\Omega_R(\mathbf{J}) + m\Omega_\phi(\mathbf{J}) - m\Omega_p, \quad (35)$$

and using (33), the condition (34) takes the convenient form

$$\mu_m^0(\mathbf{J}) \approx \mathcal{O}(\epsilon e^{st}), \quad (36)$$

which is the definition of the CR. The ILR and OLR occur if  $|\mu_m^l|$  diminishes for  $l = -1$  and  $l = 1$ , respectively.

A graphical representation of (36) will help to sharpen our understanding of the ensemble of stars that can support a rotating pattern. Since there is a one-to-one, onto and invertible map  $\mathbf{J} \rightarrow \Omega$  for initially axisymmetric disks (excluding Keplerian and harmonic oscillator potentials), any functional form of the actions can be described in terms of  $\Omega$  as well. For instance, one may write  $\mu_m^0(\mathbf{J}) \equiv \mu_m^0(\Omega)$ . I therefore identify resonant regions in the frequency space. For demonstrating the distribution of dependent quantities, I will use the pair  $(\Omega_R, \Omega_i)$  as the coordinates where  $\Omega_i = \Omega_\phi - \frac{1}{2}\Omega_R$ . The reason for this choice is that the orbital frequencies of soft-centered stellar disks fill a very narrow region in the  $\Omega$ -space (Hunter 2002, hereafter H02; Figure 1 in JH), which does not provide enough resolution for the visual identification of some fine structures. Denoting  $\Omega_0 = [\Omega_\phi]_{\text{max}}$  in a cored stellar disk, the center of the disk and infinity correspond to  $(\Omega_R, \Omega_i) = (2\Omega_0, 0)$  and  $(\Omega_R, \Omega_i) = (0, 0)$ , respectively. Figure 3 shows the frequency space of the cored logarithmic potential. The lower boundary ( $\Omega_R$ -axis) corresponds to radial orbits with  $J_\phi = 0$  and the upper curved boundary  $\Omega_i = \Gamma_c(\Omega_R)$  is determined by the orbital frequencies of circular orbits with  $J_R = 0$ .

I have plotted in Figure 3 the contours of  $|\mu_m^0(\Omega)|$  for  $m = 2$  and  $\Omega_p = 0.454\Omega_0$ , which is the pattern speed of mode S2. Lighter regions mark the stars that are closer to the exact CR. The intersection of the straight line

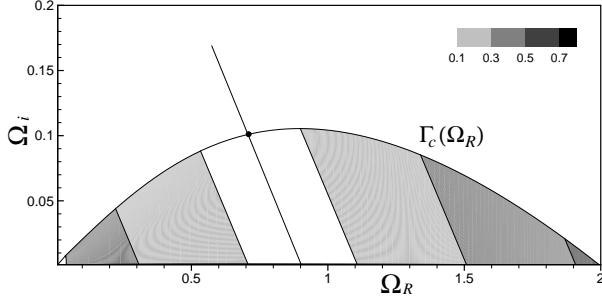


FIG. 3.— The frequency space of the cored logarithmic potential with  $R_C = v_0 = \Omega_0 = 1$ . The upper boundary  $\Omega_i = \Gamma_c(\Omega_R)$  corresponds to circular orbits with  $J_R = 0$ . Contours show the variation of the CR indicator  $|\mu_2^0(\Omega)|$  over the frequency space for  $\Omega_p = 0.454$ . Lighter regions correspond to smaller values of  $|\mu_2^0(\Omega)|$ . The function  $\mu_2^0(\Omega) = 2(\Omega_\phi - \Omega_p)$  vanishes at the intersection of the drawn straight line and the frequency space. The star at the intersection of the line  $\mu_2^0(\Omega) = 0$  and the upper boundary moves on the corotation circle.

$\mu_2^0(\Omega) = 0$  with the frequency space corresponds to the stars at the CR. The centerline of the CR zone begins at the location of a star moving on the corotation circle, and extends into inner regions.

By decreasing  $\Omega_p$ , the CR zone is pushed to the outskirts of the disk where orbital frequencies are small and the surface density has dropped substantially. Furthermore, the line  $\mu_m^0(\Omega) = 0$  will not intersect the frequency space, and there will not be a CR if  $\Omega_p > \Omega_0$ . For a similar reason, the ILR will be absent if

$$\Omega_p > \Omega_{\text{ILR}}(m), \quad (37)$$

$$\Omega_{\text{ILR}}(m) = \left[ \Gamma_c(\Omega_R) + \left( \frac{m}{2} - 1 \right) \Omega_R \right]_{\text{max}}. \quad (38)$$

Inequality (37) is satisfied when the line  $\mu_m^{-1}(\Omega) = 0$  does not cross the boundary curve  $\Omega_i = \Gamma_c(\Omega_R)$ . These properties appear to correlate with the computed eigenfrequencies of unstable modes: according to the eigen-spectra of Paper I, the pattern speeds of growing modes lie in the interval

$$\Omega_{\text{ILR}}(m) < \Omega_p < \Omega_0. \quad (39)$$

The lower limit may be violated by cold disks and disks with inner cutouts (see §7.2). The upper limit is violated by some rapidly rotating modes in galaxies with dark matter, and by mode B1 of cutout disks. After exploring the orbital structure of perturbed disks in §5, I will explain the constraint (39) and the exceptional cases that may not satisfy it.

## 5. STELLAR DYNAMICS IN THE PERTURBED DISK

The orbital dynamics of stars can be understood through investigating the induced dynamics by each Fourier component. We usually split the phase space to several subspaces by using a Fourier expansion in  $\theta_R$ , and each subspace is associated with a pattern component (e.g., Figure 2). In the linear regime, the perturbed motion of stars due to the  $l$ th component can be traced by carrying out a canonical transformation

$$(\theta_R, \theta_\phi, J_R, J_\phi) \rightarrow (w_1, w_2, I_1, I_2), \quad (40)$$

defined by the generating function (Lynden-Bell 1993)

$$\mathcal{S} = (l\theta_R + m\theta_\phi - m\Omega_p t) I_1 + \theta_R I_2. \quad (41)$$

This yields the transformation rules

$$\mathbf{w} = \frac{\partial \mathcal{S}}{\partial \mathbf{I}}, \quad \mathbf{J} = \frac{\partial \mathcal{S}}{\partial \Theta}, \quad (42)$$

and the new Hamiltonian

$$\mathcal{K} = \mathcal{H}_0(\mathbf{I}) + \mathcal{H}_1(\mathbf{w}, \mathbf{I}, t) + \partial \mathcal{S} / \partial t, \quad (43)$$

so that

$$\begin{aligned} \mathcal{K} &= \mathcal{H}_0(\mathbf{I}) - m\Omega_p I_1 \\ &+ \epsilon e^{st} \text{Re} \sum_{k=-\infty}^{\infty} \sum_{j=0}^{\infty} \tilde{a}_j^m \Psi_j^{mk}(\mathbf{I}) e^{i[w_1 + (l-k)w_2]}. \end{aligned} \quad (44)$$

From the equations of motion

$$\dot{\mathbf{I}} = -\frac{\partial \mathcal{K}}{\partial \mathbf{w}}, \quad \dot{\mathbf{w}} = \frac{\partial \mathcal{K}}{\partial \mathbf{I}}, \quad (45)$$

one can verify that  $w_2 = \Omega_R t + \mathcal{O}(\epsilon e^{st})$  is an increasing function of time, which can be made a cyclic coordinate by averaging  $\mathcal{K}$  over  $w_2$ . Consequently, the action  $I_2 = J_R - lI_1 = J_R - lJ_\phi/m$  becomes an adiabatic invariant so that  $\dot{I}_2 = \mathcal{O}(\epsilon^2 e^{2st})$ , and the dynamics is reduced to the flows governed by the averaged Hamiltonian

$$\overline{\mathcal{K}}(m, l) \equiv \langle \mathcal{K} \rangle_{w_2} = \overline{\mathcal{K}}_0 + \epsilon e^{st} \overline{\mathcal{K}}_1, \quad (46)$$

$$\overline{\mathcal{K}}_0(\mathbf{I}) = \mathcal{H}_0(\mathbf{I}) - m\Omega_p I_1 \quad (47)$$

$$\overline{\mathcal{K}}_1 = A_m^l(\mathbf{I}) \cos[w_1 + \vartheta_m^l(\mathbf{I})], \quad (48)$$

where I have kept the real (physical) part of  $\langle \mathcal{K} \rangle_{w_2}$  and

$$A_m^l(\mathbf{I}) = \sqrt{X^2 + Y^2}, \quad \vartheta_m^l(\mathbf{I}) = \arctan\left(\frac{Y}{X}\right), \quad (49)$$

$$X = \sum_{j=0}^{\infty} u_j^m \Psi_j^{ml}(\mathbf{I}), \quad Y = \sum_{j=0}^{\infty} v_j^m \Psi_j^{ml}(\mathbf{I}). \quad (50)$$

The action  $I_2$  remains a constant parameter over a time scale of  $1/\mathcal{O}(\epsilon e^{st})$ .

The angle  $w_1$  can become a rotating or librating angle depending on the initial value of  $\mu_m^l(\mathbf{I})$ . Stars will be near a mean-motion resonance if  $w_1$  librates. For simplicity, I introduce the slow angle  $\theta = w_1 + \vartheta_m^l(\mathbf{I}) - \pi$ , which casts  $\overline{\mathcal{K}}(m, l)$  into the form

$$\overline{\mathcal{K}}(m, l) = \mathcal{H}_0(\mathbf{I}) - m\Omega_p I_1 - \epsilon e^{st} A_m^l(\mathbf{I}) \cos \theta. \quad (51)$$

The distribution function (DF)  $f = f_0 + f_1$  is thus conserved along the trajectories determined by

$$\dot{\theta} = \frac{\partial \overline{\mathcal{K}}(m, l)}{\partial I_1} = \mu_m^l(\mathbf{I}) - \epsilon e^{st} \frac{\partial A_m^l(\mathbf{I})}{\partial I_1} \cos \theta, \quad (52)$$

$$\dot{I}_1 = -\frac{\partial \overline{\mathcal{K}}(m, l)}{\partial \theta} = -\epsilon e^{st} A_m^l(\mathbf{I}) \sin \theta. \quad (53)$$

These are equations of perturbed orbits bound to the  $l$ th Fourier component in the linear regime. According to the dynamical mechanism presented in §4, the  $l = 0$  Fourier component is capable of keeping  $\mu_m^l(\mathbf{I}) \approx \mathcal{O}(\epsilon e^{st})$ , which in turn, can lead to the resonant capture of stars in the linear regime once  $\theta$  begins to evolve slowly.

I have frozen the (small) exponential factor  $\epsilon e^{st}$  and plotted the instantaneous isocontours (ICs) of  $\overline{\mathcal{K}}(2, 0)$  in Figure 4 for the initially circular orbits ( $I_2 = 0$ ) of

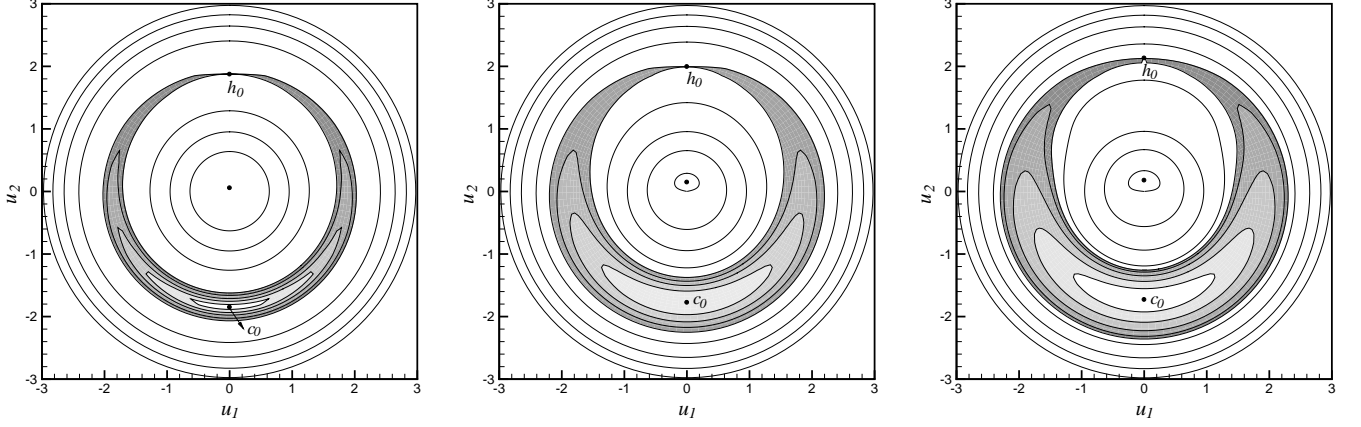


FIG. 4.— The instantaneous isocontours of the averaged Hamiltonian  $\bar{\mathcal{K}}(2,0)$  for mode S2. The factor  $\epsilon e^{st}$  is dealt with as a constant and has been set to 0.01 (left panel), 0.05 (middle panel) and 0.1 (right panel). The maximum of  $\bar{\mathcal{K}}_1$  has been normalized to unity. The crescent-like resonant zone, driven by the instantaneous elliptic point  $c_0$ , has been shaded. Darker regions correspond to smaller values of  $\bar{\mathcal{K}}(2,0)$ . The separatrices intersect at the instantaneous hyperbolic point  $h_0$ .

mode S2. The isocontours have been displayed in the coordinate plane of  $u_1 = \sqrt{2I_1} \sin \theta$  and  $u_2 = \sqrt{2I_1} \cos \theta$  where the transformation  $(\theta, I_1) \rightarrow (u_1, u_2)$  is canonical. Note that the angle  $\theta$  is measured clockwise with respect to the positive  $u_2$ -direction.

The IICs of Figure 4 resemble the topology of the celestial three-body problem (e.g., Wisdom 1980; Winter & Murray 1997). Two homoclinic loops that intersect at the instantaneous hyperbolic point  $h_0$  surround a crescent-like, resonant region where the angle  $\theta$  librates. The instantaneous elliptic point  $c_0$  corresponds to stable orbits at exact resonance. For a specified  $I_2$ , the coordinates of  $c_0$  and  $h_0$  are  $(\theta, I_1) = [\pi, r_\pi(t)]$  and  $(\theta, I_1) = [0, r_0(t)]$ , respectively, where  $r_\pi(t)$  and  $r_0(t)$  are the real roots of

$$\mu_m^0(r_z, I_2) - \epsilon e^{st} \frac{\partial A_m^0(r_z, I_2)}{\partial r_z} \cos z = 0, \quad z = 0, \pi, \quad (54)$$

at a given time  $t$ .

To this end, I show that the elliptic point  $c_0$  always lies on the negative  $u_2$ -axis with  $\theta = \pi$ . I assume the small variations  $\tilde{\theta} = \theta - \pi$  and  $\tilde{I}_1 = I_1 - r_\pi(t)$  for  $l = 0$ , and linearize equations (52) and (53) to obtain

$$\frac{d\tilde{\theta}}{dt} = a_{12}(t) \tilde{I}_1, \quad (55)$$

$$\frac{d\tilde{I}_1}{dt} = a_{21}(t) \tilde{\theta} - \dot{r}_\pi(t), \quad (56)$$

where the time-dependent coefficients are defined as

$$a_{12}(t) = \left[ \frac{\partial \mu_m^0(\mathbf{I})}{\partial I_1} + \epsilon e^{st} \frac{\partial^2 A_m^0(\mathbf{I})}{\partial I_1^2} \right]_{I_1=r_\pi(t)}, \quad (57)$$

$$a_{21}(t) = \epsilon e^{st} [A_m^0(\mathbf{I})]_{I_1=r_\pi(t)}. \quad (58)$$

The quantity  $\dot{r}_\pi(t)$  is determined by differentiating (54) with respect to  $t$ . I obtain

$$\dot{r}_\pi(t) = -\frac{a_{13}(t)}{a_{12}(t)}, \quad (59)$$

$$a_{13}(t) = \epsilon s e^{st} \left[ \frac{\partial A_m^0(\mathbf{I})}{\partial I_1} \right]_{I_1=r_\pi(t)}. \quad (60)$$

Eliminating  $\tilde{I}_1$  from the linearized equations leads to

$$\frac{d^2 \tilde{\theta}}{dt^2} + a_0(t) \tilde{\theta} = a_{13}(t) + \mathcal{O}(\epsilon^2 e^{2st}), \quad (61)$$

$$a_0(t) = - \left[ \epsilon e^{st} A_m^0(\mathbf{I}) \frac{\partial \mu_m^0(\mathbf{I})}{\partial I_1} \right]_{I_1=r_\pi(t)}. \quad (62)$$

The sign of the time-dependent *spring coefficient*  $a_0(t)$  is determined by the sign of  $\partial \mu_m^0 / \partial I_1$ . In cored stellar disks whose equilibrium potential fields are monotonic functions of  $R$ , the following conditions always hold

$$\frac{\partial \Omega_R(\mathbf{J})}{\partial J_\phi} \leq 0, \quad \frac{\partial \Omega_\phi(\mathbf{J})}{\partial J_\phi} \leq 0. \quad (63)$$

The equality sign corresponds to the galactic center. The isochrone, Kuzmin-Toomre and cored exponential disks (investigated in JH and Paper I) fulfill (63), which implies  $\partial \mu_m^0 / \partial I_1 < 0$ . Therefore, the spring coefficient  $a_0(t)$  is positive and the homogeneous solution of (61) is bounded. This proves that the instantaneous critical point  $(\theta, I_1) = [\pi, r_\pi(t)]$  is of elliptic type.

The resonant zone disappears for  $l \neq 0$  when the pattern speed lies in the interval (39). This is because all participating stars in the pattern formation satisfy (36) that yields

$$\mu_m^l(\mathbf{I}) \approx l \Omega_R + \mathcal{O}(\epsilon e^{st}). \quad (64)$$

Accordingly,  $\mu_m^l(\mathbf{I})$  cannot flip sign for  $l \neq 0$  and equation (54) will not have any real root for small perturbations of  $\mathcal{O}(\epsilon e^{st})$ . In such a circumstance, IICs will constitute a bundle of unidirectional closed curves that encircle the origin. In §5.3, I will verify for the spiral mode S2 that pattern stars satisfy (64).

### 5.1. The Expansion of Resonant Zones

It is evident that the structure of IICs in Figure 4 evolves with time as the perturbations grow proportional to  $\epsilon e^{st}$ . For small perturbations the critical points  $c_0$  and  $h_0$  are preserved although they are displaced. As a consequence, there always exists a resonant zone for  $\epsilon e^{st} \ll 1$  and it would be interesting to learn how that

zone *expands* in a growing mode. To answer this question analytically, I measure the variation of the quantity

$$\Delta = d_o - d_i, \quad (65)$$

where  $d_o$  and  $d_i$  are, respectively, the values of  $I_1$  on the outer and inner homoclinic loops at  $\theta = \pi$ . The implicit functional form of homoclinic loops is given by

$$\begin{aligned} \bar{\mathcal{K}}_0(I_1, I_2) - \epsilon e^{st} A_m^0(I_1, I_2) \cos \theta = \\ \bar{\mathcal{K}}_0[r_0(t), I_2] - \epsilon e^{st} A_m^0[r_0(t), I_2], \end{aligned} \quad (66)$$

whose temporal derivative at  $\theta = \pi$  results in

$$\begin{aligned} \dot{d}_\nu \left[ \mu_m^0 + \epsilon e^{st} \frac{\partial A_m^0}{\partial I_1} \right]_{I_1=d_\nu} + \epsilon s e^{st} A_m^0(d_\nu, I_2) = \\ \dot{r}_0 \left[ \mu_m^0 - \epsilon e^{st} \frac{\partial A_m^0}{\partial I_1} \right]_{I_1=r_0} - \epsilon s e^{st} A_m^0(r_0, I_2), \end{aligned} \quad (67)$$

for  $\nu \equiv o, i$ . The bracket on the right hand side of equation (67) vanishes because of (54) and the bracket on the left hand side is simply  $d\theta_\nu/dt$  ( $\nu=o, i$ ). From (52) and (53) one can verify that  $d\theta_o/dt < 0$  and  $d\theta_i/dt > 0$ . Equation (67) thus becomes

$$\dot{d}_\nu = -\frac{\epsilon s e^{st}}{\dot{\theta}_\nu} [A_m^0(d_\nu, I_2) + A_m^0(r_0, I_2)], \quad \nu \equiv o, i. \quad (68)$$

Subtracting  $\dot{d}_i$  from  $\dot{d}_o$  leads to

$$\begin{aligned} \dot{\Delta} = s (\epsilon e^{st}) \left[ \frac{A_m^0(d_o, I_2)}{|\dot{\theta}_o|} + \frac{A_m^0(d_i, I_2)}{|\dot{\theta}_i|} \right. \\ \left. + \frac{A_m^0(r_0, I_2)}{|\dot{\theta}_o|} + \frac{A_m^0(r_0, I_2)}{|\dot{\theta}_i|} \right]. \end{aligned} \quad (69)$$

The angular rates  $\dot{\theta}_o$  and  $\dot{\theta}_i$  can be estimated using the linearized equation (55) as

$$\dot{\theta}_o = a_{12}(t) [d_o - r_\pi(t)], \quad \dot{\theta}_i = a_{12}(t) [d_i - r_\pi(t)]. \quad (70)$$

Since the resonant zone is thin, one may assume  $r_\pi(t) \approx (d_o + d_i)/2$ , which can be combined with (70) to obtain

$$|\dot{\theta}_o| \approx |\dot{\theta}_i| \approx |a_{12}(t)| \frac{\Delta}{2}. \quad (71)$$

Substituting from (71) in (69) yields

$$\begin{aligned} \Delta \dot{\Delta} \approx \frac{2s (\epsilon e^{st})}{|a_{12}(t)|} \left[ 2A_m^0(r_0, I_2) \right. \\ \left. + A_m^0(d_i, I_2) + A_m^0(d_o, I_2) \right], \end{aligned} \quad (72)$$

where the quotient of the bracketed terms and  $|a_{12}(t)|$  is of  $\mathcal{O}(1)$ . Integrating (72) results in

$$\Delta \approx 2\sqrt{\epsilon e^{st}} \mathcal{O}(1), \quad \dot{\Delta} \approx s\sqrt{\epsilon e^{st}} \mathcal{O}(1), \quad (73)$$

from which the expansion rate of the resonance width per unit length is estimated:

$$\dot{\Delta}/\Delta \sim s/2. \quad (74)$$

This shows that stars are steadily captured into resonance by the  $l = 0$  Fourier component as the mode grows in the linear regime.

My calculations show that the maximum of  $A_m^0(\mathbf{I})$  in unstable modes does not coincide neither with  $h_0$  nor with  $c_0$ , but it falls inside the resonant zone within a time scale  $\ll 1/\mathcal{O}(\epsilon e^{st})$  as  $\Delta$  grows from zero width. The observed shift from the location of  $c_0$  depends on the gradient  $\partial f_0/\partial J_\phi$ . All growing modes obey the following rules near  $c_0$ :

$$\frac{\partial A_m^0(\mathbf{I})}{\partial I_1} < 0 < \mu_m^0(\mathbf{I}) \quad \text{if} \quad \frac{\partial f_0(\mathbf{J})}{\partial J_\phi} < 0, \quad (75)$$

$$\frac{\partial A_m^0(\mathbf{I})}{\partial I_1} > 0 > \mu_m^0(\mathbf{I}) \quad \text{if} \quad \frac{\partial f_0(\mathbf{J})}{\partial J_\phi} > 0. \quad (76)$$

In both cases the magnitude of  $\mu_m^0(\mathbf{I})$  remains small near the maximum of  $A_m^0(\mathbf{I})$ , confirming the theory of §4 that the perturbed density profile is supported by the synchronous precession of orbital axes.

## 5.2. Angular Momentum Transfer

The location of the resonant zone in the  $(u_1, u_2)$ -plane provides valuable information of the behavior of resonant stars. The Hamiltonian varies according to the equation

$$\frac{d\bar{\mathcal{K}}(m, l)}{dt} = \frac{\partial \bar{\mathcal{K}}(m, l)}{\partial t} = -\epsilon s e^{st} A_m^l(\mathbf{I}) \cos \theta. \quad (77)$$

One can thus determine how the orbital energy of trapped stars changes over time. Recalling that the instantaneous elliptic point  $c_0$  occurs at  $\theta = \pi$ , for most resonant orbits the minimum of  $\theta$  is larger than  $\pi/2$  (see Figure 4) and equation (77) yields

$$\frac{d\bar{\mathcal{K}}(m, 0)}{dt} > 0. \quad (78)$$

In other words, stars gain energy during a librational motion around  $\theta = \pi$ . Since  $I_2 = J_R$  (for  $l = 0$ ) is an adiabatic invariant in the resonance zone, an increase in the orbital energy of stars boosts their angular momentum.

There is a different mechanism for the angular momentum transfer to/from stars whose  $\theta$  is rotational. Such stars will definitely experience both  $\dot{I}_1 > 0$  and  $\dot{I}_1 < 0$  states over a complete period of  $\theta$ , but which one overwhelms the other and how does it affect the orbital angular momentum? Outside the resonant zone we have

$$|\mu_m^l(\mathbf{I})| \gg \left| \epsilon e^{st} \frac{\partial A_m^l(\mathbf{I})}{\partial I_1} \right|, \quad (79)$$

which guarantees the rotation of  $\theta$  according to (52). I now divide equation (53) by (52) and ignore all terms of  $\mathcal{O}(\epsilon^2 e^{2st})$  to obtain

$$\frac{dI_1}{d\theta} = -\frac{\epsilon}{\mu_m^l(\mathbf{I}_0)} \exp \left[ \frac{s\theta}{\mu_m^l(\mathbf{I}_0)} \right] A_m^l(\mathbf{I}_0) \sin \theta, \quad (80)$$

where  $\mathbf{I}_0$  is the initial value of the action vector  $\mathbf{I} = (I_1, I_2)$  at  $\theta = 0$ . For a clockwise rotation of phase space flows,  $\theta$  ranges from 0 to  $2\pi$  and reversely for their counter-clockwise rotation. Moreover, the direction of rotation is determined by the sign of  $\mu_m^l(\mathbf{I}_0)$ . Given these points, integrating (80) over a complete cycle of  $\theta$  results in the incremental change of  $I_1$  as

$$\Delta I_1(l) = \epsilon A_m^l \frac{\mu_m^l \text{sign}(\mu_m^l)}{(\mu_m^l)^2 + s^2} \left[ \exp \left( \frac{2\pi s}{\mu_m^l} \right) - 1 \right]. \quad (81)$$



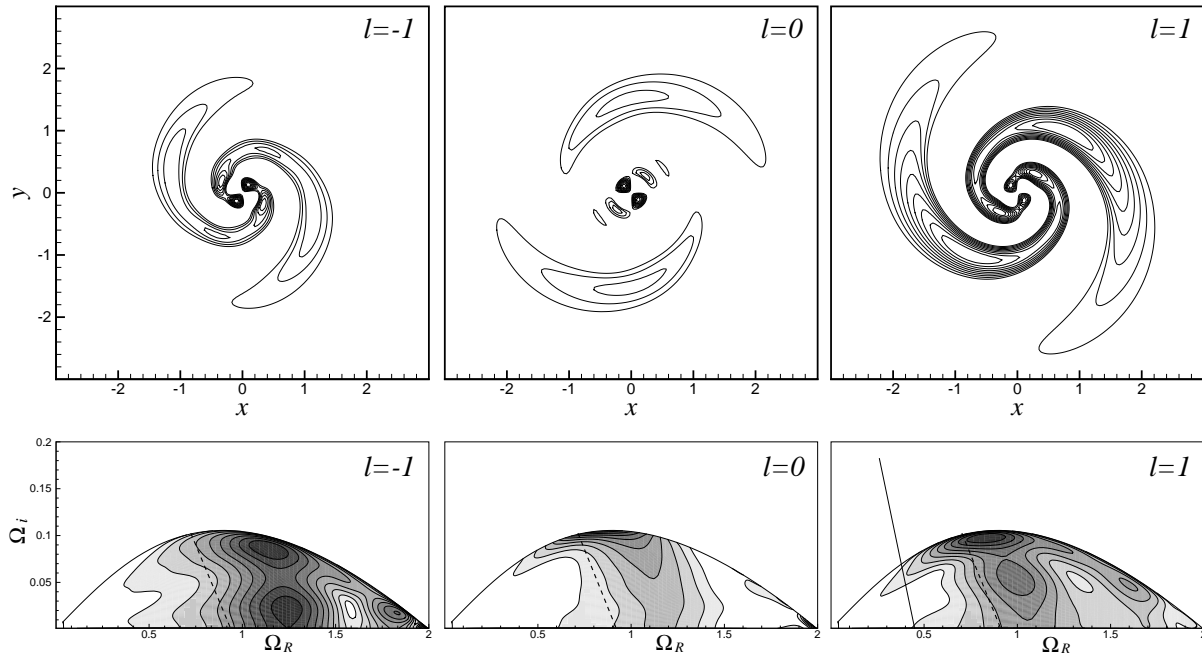


FIG. 5.— The density components  $\Sigma_1^l$  (top panels) and the contours of  $A_2^l(\Omega)$  (bottom panels) for mode S2. In all figures dashed lines mark the stars at exact CR with  $\mu_2^0(\Omega) = 0$ . The line  $\mu_2^{-1}(\Omega) = 0$  lies outside the plot range because it is parallel to the  $\Omega_R$ -axis with  $\Omega_i = 0.454$ . Straight solid line in the bottom-right panel is defined by  $\mu_2^1(\Omega) = 0$ . Its relative location with respect to the highly populated regions of the frequency space shows that stars bound to the  $l = 1$  component evolve far from the OLR. The contour levels of  $A_2^l(\Omega)$  range from 10% to 90% of the maximum with increments of 10%.

It is seen that  $\Delta I_1$  is positive for  $\mu_m^l(I_0) > 0$  and stars gain angular momentum as the perturbations grow. The opposite happens for  $\mu_m^l(I_0) < 0$ . Combining (64) and (81) shows that the angular momentum gain or loss is decided by the sign and magnitude of the Fourier number  $l$ . The Fourier components with  $l < 0$  and  $l > 0$  respectively drain and boost the angular momentum of stars so that

$$\Delta I_1(-1) < \Delta I_1(-2) < \Delta I_1(-3) < \dots < 0, \quad (82)$$

$$\Delta I_1(+1) > \Delta I_1(+2) > \Delta I_1(+3) > \dots > 0. \quad (83)$$

Not all stars bound to the  $l = 0$  component are in the resonant zone, specially in the limit of  $\epsilon e^{st} \rightarrow 0$ . Hence, the sign of  $\Delta I_1(0)$  is determined both by resonant and non-resonant stars. Based on my arguments presented after equation (77), resonant stars always gain angular momentum and have a positive contribution to  $\Delta I_1(0)$ . However, it is the sign of  $\partial f_0 / \partial J_\phi$  that determines whether non-resonant stars of the  $l = 0$  component are emitting or absorbing angular momentum. Equations (75) and (76) together with (81) show that non-resonant stars of the  $l = 0$  component gain and lose angular momentum for  $\partial f_0 / \partial J_\phi < 0$  and  $\partial f_0 / \partial J_\phi > 0$ , respectively. Therefore,  $\Delta I_1(0)$  is certainly positive if the mode develops in a region of the phase space with  $\partial f_0 / \partial J_\phi < 0$ . Since most stars of the  $l = 0$  component are non-resonant as  $\epsilon e^{st} \rightarrow 0$ , the occurrence of a growing mode as a result of  $\partial f_0 / \partial J_\phi > 0$  will lead to  $\Delta I_1(0) < 0$ . The results of the above analysis are consistent with the results of JH and the bar charts of Figure 1.

### 5.3. Mode Components in the Frequency Space

To understand how the mechanism of resonant trapping operates on non-circular orbits in the frequency

space, I have plotted the components of mode S2 in Figure 5. Top panels display the pattern components in the configuration space, and in bottom panels I have shown the isocontours of  $A_2^l(\Omega) \equiv A_2^l(I)$  together with the lines  $\mu_2^l(\Omega) = 0$  (straight solid line) and  $\mu_2^0(\Omega) = 0$  (dashed lines). Darker regions in the bottom panels correspond to larger values of  $A_2^l(\Omega)$ . The contour plots of  $A_2^l(\Omega)$  show which stars in the frequency/action space are engaged with the  $l$ th component. As one could anticipate, the highly populated regions of all components are close to the CR zone of Figure 3. The maxima of  $A_2^l(\Omega)$  have not been located on the line  $\mu_2^0(\Omega) = 0$  because the initial density gradient of the equilibrium state displaces the center of mass of pattern stars. In modes with  $\partial f_0 / \partial J_\phi < 0$  near the CR zone, the maxima are shifted to regions with  $\mu_2^0(\Omega) > 0$  (see §5.1).

Whilst the  $l = 0$  component has trapped near-circular orbits into the CR (Figure 5), the stars bound to other components evolve far from mean-motion resonances and the angle  $\theta$  becomes rotational for them. In fact, stars bound to the  $l = -1$  component avoid the line  $\mu_m^{-1}(\Omega) = 0$  and the quantity  $\mu_m^{-1}(\Omega)$  is always negative as long as inequality (37) holds. Through a similar mechanism, stars avoid the line  $\mu_m^1(\Omega) = 0$  and the quantity  $\mu_m^1(\Omega)$  remains positive regardless of the magnitude of  $\Omega_p$ . These results show that the dynamical mechanism for growing modes of finite  $s$  differs with LBK's theory established in the limit of  $s \rightarrow 0$ . In other words, in a growing spiral mode similar to mode S2 of this paper, the  $l = -1$  and  $l = 1$  components are not associated with the ILR and OLR. A new dynamical origin of instabilities, which interprets the results of this paper and has not the restrictions of LBK's theory, is presented in the

next section.

## 6. THE ORIGIN OF INSTABILITIES

Consider a randomly generated, small-amplitude,  $m$ -fold density wave of pattern speed  $\Omega_p$  whose potential field can be generally expanded in the Fourier series of the angle variables. Independent of the form of initial phase space distribution, determined by  $f_0(\mathbf{J})$ , the points  $(\mathbf{I}, \theta) = (\mathbf{I}_0, 0)$  and  $(\mathbf{I}, \theta) = (\mathbf{I}_0, \pi)$  will emerge as time-invariant stationary points of the flows generated by  $\overline{\mathcal{K}}(m, 0)$  if the following condition holds

$$\frac{\partial A_m^0(\mathbf{I})}{\partial I_1} = \mu_m^0(\mathbf{I}) = 0, \quad (84)$$

at  $\mathbf{I} = \mathbf{I}_0$ . In such a circumstance, orbits associated with either of these stationary points will never change their action vector  $\mathbf{I} = (I_1, I_2)$  and their orbital energy must be conserved. This condition will be satisfied only if  $s = 0$  in (77). This is how a van Kampen (1955) mode is born. The state of (84) can occur at any point in the infinite dimensional action space and for arbitrary values of  $\Omega_p$ . Consequently, stationary modes constitute a continuous family and Mathur's (1990) isolated, pure oscillatory modes are not feasible in stellar disks.

Let me now suppose that for some pattern speed  $\Omega_p$  in the interval (39), the quantity  $\mu_m^0(\mathbf{I})$  accidentally remains small (for a group of stars) over a finite duration of time, but the condition (84) is violated. This (likely) symmetry-breaking phenomenon creates a slim resonant zone of the width  $\Delta(t)$  (see §5.1). There is not any physical constraint on the evolution of  $\Delta(t)$  when the perturbations are in their early stages. For a steady rate given by (74) more stars are trapped by the resonant zone if  $s > 0$  and the density wave corresponding to the Fourier number  $l = 0$  is magnified. As I discussed in §5.2, the angular momentum of the captured stars increases and some other *reacting stars* should therefore respond in order to recover the angular momentum balance of the disk. The reacting stars live in the same CR zone defined by  $\mu_m^0(\mathbf{I}) \approx \mathcal{O}(\epsilon \epsilon^{st})$ .

As more stars are trapped into resonance by the  $l = 0$  component, non-resonant components with  $|l| > 0$  should also involve more stars to compensate the angular momentum deficit. So the amplitudes of other wave components increase as well. This is what I am considering as the origin of instabilities: triggering unsteady density perturbations by the capture of stars into the CR. Angular momentum transfer between non-resonant stars cannot be facilitated if a resonant gap does not open in the phase space. In fact, the initial destabilizing imbalance of  $\mathcal{L}$  is generated by an irreversible engagement of resonant stars even if the amount of angular momentum that they absorb is small (e.g., Figure 8 in JH). A perturbation with the property of (84) fixes  $s = 0$ , does not awake stars of  $|l| > 0$  components, and it creates a stationary mode. I conclude that most (if not all) unstable modes disappear for  $\Omega_p > \Omega_0$  just because the CR is destroyed in such a circumstance.

The  $l = 0$  component is not always an angular momentum absorber. For example, in models with an inner cutout of the DF, one has  $\partial f_0 / \partial J_\phi > 0$  which enforces  $L_m(0) < 0$  (discussions in §5.2 and JH). Figures 2 and 11 in JH demonstrate two modes that show angular mo-

mentum emission by the  $l = 0$  component. The pattern speeds of some C-modes explored in Paper I exceed  $\Omega_0$  marginally. Those modes also have  $L_m(0) < 0$ . Unstable modes with  $\Omega_p > \Omega_0$  are barely observed in modal calculations because their large pattern speeds shrink them to the galactic center. Coexistence of mode B1 and a compact C-mode can explain the origin of double-barred galaxies. For a softened-gravity model of the exponential disk with an inner cutout, Alar Toomre (private communication) also finds an inner edge mode that has a corotation circle inside its pattern. Toomre's inner edge mode is another example of a mode with  $\partial f_0 / \partial J_\phi > 0$  and  $L_m(0) < 0$ . Axisymmetric features/grooves introduced by Sellwood & Kahn (1991) to the surface density and DF also develop a spiral mode whose pattern is discontinuous at the location of the groove. That discontinuity is due to the rapid change in the sign of  $\partial f_0 / \partial J_\phi$ : while the  $l = 0$  component boosts the angular momentum of stars outside the groove, it has an opposite effect on inner stars.

Each unstable mode occupies a finite region in the frequency space due to the finiteness of its CR zone. This is how divisions (gaps) are created between the pattern speeds of unstable modes, the  $\Omega$ -space is quantized by resonances, and finally, unstable modes constitute a discrete family. Growth rates are sorted according to the likelihood of resonant capture, which is proportional to the initial population of stars determined by the equilibrium DF. In a stellar disk with a falling density profile, the growth rates of linear modes are sorted in a decreasing order from compact modes to more extensive ones. Most barred and spiral modes obey this rule (see Paper I). The perturbation theory of §5 says that stars live on the integral manifolds of constant  $I_2$  before and after capture into resonance. In order to guarantee a sustained growth of the CR zone, the initial DF  $f_0(\mathbf{J})$  must be smooth and non-zero along the curves of constant  $I_2$ , and  $\mu_m^0(\mathbf{I})$  has to flip its sign there. A resonant zone cannot grow in a region of the phase space which is devoid of stars from the beginning, or its stars have been forced to migrate by unsteady processes. The first-order perturbation theory is valid as long as the CR zone of each mode is inaccessible by the stars of other modes and  $I_2$  is an adiabatic invariant.

## 7. MODE SATURATION AND STABLE DISKS

Perhaps the most important issue related to the growth of instabilities is that the amplitudes of unstable modes are saturated after several pattern rotations. Saturation is indeed a nonlinear phenomenon and can have complex routes. Sellwood & Binney (2002) suggest that the growth of a mode is stopped by the emergence of horseshoe orbits. What they call "horseshoe orbits" are simply the librational orbits captured by the CR. I found those orbits the main cause of instabilities. I agree with Sellwood & Binney (2002) that the linear perturbation theory must fail at some stage, but it does not necessarily imply that resonant zones can self-control their expansion beyond the linear regime. Using the phase space geometry and the nonexistence of the first integral  $I_2$  at the boundaries of neighboring resonances, I argue that resonance overlapping is an alternative and efficient mechanism to stop the growth of unstable modes. The stabilization of stellar disks in the presence of the ILRs is also

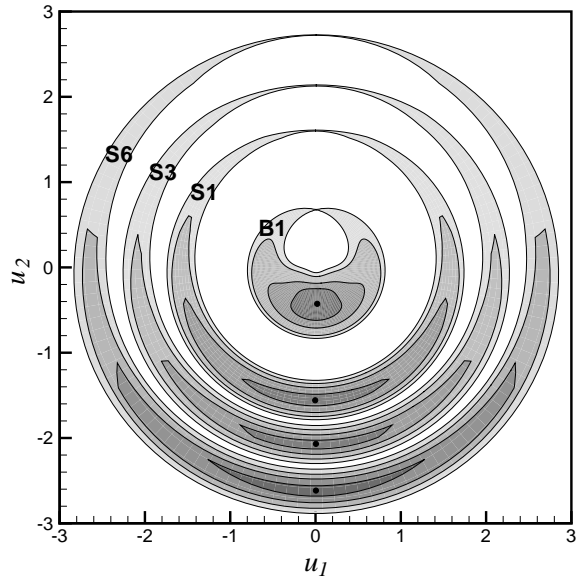


FIG. 6.— The resonant zones of modes B1, S1, S3 and S6 for the cored exponential disk with  $(N, \lambda, \alpha) = (6, 1, 0.42)$ . Contour plots show the IICs of  $\bar{\mathcal{K}}(2, 0)$  for  $I_2 = 0$  and  $\epsilon e^{st} = 0.01$ . Darker regions correspond to larger values of  $\bar{\mathcal{K}}(2, 0)$ . Contour levels of each zone have been normalized to the maximum value of  $\bar{\mathcal{K}}(2, 0)$  in the same zone.

explained by the same mechanism. I then present a simple criterion for the stability of non-axisymmetric perturbations, and discuss about the stability of self-consistent scale-free disks.

### 7.1. Resonance Overlapping

As a mode grows, the width of its CR zone increases proportional to  $\sqrt{\epsilon e^{st}}$  until two adjacent zones, corresponding to modes of different pattern speeds, overlap and compete for trapping the stars in the overlapping zone. This is the moment that a chaotic layer occurs in the phase space according to Chirikov's (1979) theory, and stars living in that layer repeatedly migrate between different resonant zones. Thus, the share contributed to each competing resonant zone from stars in the overlapping region drops substantially and the growth is suppressed. A natural consequence of the emergence of a chaotic layer is the radial migration of stars that heats up the disk. Some modes may be gradually dissolved as their Kolmogorov-Arnold-Moser (KAM) tori around stable periodic orbits are destroyed by modes with larger resonant zones and growth rates. I remark that the weighted residual form of the CBE that I obtained in Paper I is valid as long as we are allowed to average out angle variables from dynamical equations. After the occurrence of chaotic orbits it is impossible to average out resonant angles and extra coupling terms between the amplitudes of unstable modes are contributed to the reduced CBE. Details of my numerical simulations in the nonlinear regime and in the presence of chaotic orbits will be presented in Paper III.

Figure 6 shows the  $l = 0$  resonant zones of modes B1, S1, S3, and S6 for the initially circular orbits ( $I_2 = 0$ ) of the model introduced in §2. This is the first demonstration of its kind that shows how the resonant zones of different unstable modes partition the phase space of a

stellar disk. Since the perturbations grow according to an exponential law, resonant zones had been slim rings infinitely long ago. The structure shown in Figure 6 has been obtained by setting  $\epsilon e^{st} = 0.01$  for all modes. Correspondingly, resonant gaps are of comparable size at the displayed moment but they will not remain so because the growth rates are different. Left panel in Figure 7 shows the amplitude function  $A_2^0(\Omega)$  of the same modes of Figure 6 but this time in the frequency space that covers all possible values of  $I_2$ . Arrows indicate the expansion direction of the  $l = 0$  Fourier component as the modes grow. The growth rates of modes are different and mode S6, which is at the bifurcation point of the S-family (see Figure 2a in Paper I), has the smallest  $s$ . The configuration of the CR zones in the phase/frequency space and their thickening according to equation (74) suggest that resonance overlapping is likely in stellar disks with rich branches of unstable modes in their eigenspectra.

To find out how and when an overlap takes place, I assume two growing waves with the eigenvalues  $m\Omega_{p,1} + is_1$  and  $m\Omega_{p,2} + is_2$  that successively appear in the spectrum with  $\Omega_{p,1} > \Omega_{p,2}$ . These waves develop CR zones of widths  $\Delta_1(I_2)$  and  $\Delta_2(I_2)$  on each manifold of constant  $I_2$ , and I define  $d_{12}(I_2)$  as the distance between the instantaneous elliptic points of those zones. Let me suppose that the global minimum of  $d_{12}(I_2)$  corresponds to the critical action  $I_2 = I_2^{\text{cr}}$ . An overlap thus occurs if

$$d_{12}(I_2^{\text{cr}}) \lesssim \frac{1}{2} [\Delta_1(I_2^{\text{cr}}) + \Delta_2(I_2^{\text{cr}})]. \quad (85)$$

On the other hand, the magnitude of  $d_{12}(I_2^{\text{cr}})$  can be estimated as

$$d_{12}(I_2^{\text{cr}}) \approx I_{1,2} - I_{1,1} + \mathcal{O}(\epsilon e^{st}), \quad (86)$$

where  $\Omega_\phi(I_{1,j}, I_2^{\text{cr}}) = \Omega_{p,j}$  ( $j=1,2$ ). By combining (85) and (86), and using (73), I obtain

$$I_{1,2} - I_{1,1} \lesssim \left[ \sqrt{\epsilon e^{s_1 t}} \mathcal{O}_1(1) + \sqrt{\epsilon e^{s_2 t}} \mathcal{O}_2(1) \right]_{I_2=I_2^{\text{cr}}}, \quad (87)$$

which will be satisfied in the linear regime at some  $t = t_{\text{cr}}$  for a sufficiently small value of  $I_{1,2} - I_{1,1}$ . If the post-linear changes in the DF allow for a sustained expansion of resonant zones (when the amplitude growth is no longer exponential), one can still anticipate an overlap for larger values of  $I_{1,2} - I_{1,1}$ . Cooling a stellar disk increases the number of unstable modes (Figure 6 in Paper I) and decreases the gaps between the CR zones. Consequently, transition to chaos is faster in cold disks than hot ones. This result is in harmony with Sellwood's (2007, private communication)  $N$ -body experiments. The very first overlapping does not necessarily occur between the modes of the same azimuthal wavenumber  $m$ . The pattern speeds of two rapidly growing modes of different  $m$  may result in a very small  $I_{1,2} - I_{1,1}$  and thus cause an early-stage overlap.

The fundamental bar mode may still be saturated in the absence of spiral modes and in a shorter time scale than chaotic diffusion of stars. When the resonant zone of mode B1 grows, the inner homoclinic loop rapidly shrinks to central regions, the supply of stars to the CR zone is cut from the galactic center, and the bar mode saturates there. On the other hand, the bar continues to elongate because of the expansion of the outer homo-

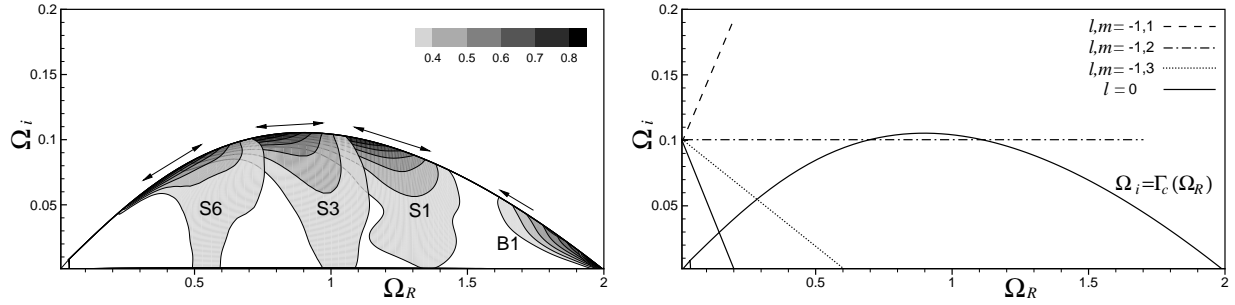


FIG. 7.— *Left panel:* Contour plots of  $A_2^0(\Omega)$  for modes B1, S1, S3 and S6 of the cored exponential disk with  $(N, \lambda, \alpha) = (6, 1, 0.42)$ . The levels of isocontours have been normalized to the maximum amplitude. *Right panel:* The emergence of ILR through the intersection of the lines  $\mu_m^{-1}(\Omega) = 0$  with the frequency space. The line  $\mu_m^0(\Omega) = 0$  (it is independent of  $m$ ) has also been plotted to show the location of the CR. In all cases the pattern speed has been set to  $\Omega_p = 0.1$ . There is no ILR associated with  $m = 1$  perturbations for any  $\Omega_p > 0$ .

clinic loop. The elongation rate, however, will slow down if  $\partial f_0 / \partial J_\phi < 0$ . A declining rate of amplitude growth gives time to the trapped stars to fill their invariant tori and maintain the bar in outer regions.

### 7.2. The Role of Inner Lindblad Resonances

Disappearance of unstable modes when the pattern speed violates (37) can also be explained by the same mechanism that saturates instabilities. The ILR emerges when the line  $\mu_m^{-1}(\Omega) = 0$  crosses the circular orbit boundary  $\Omega_i = \Gamma_c(\Omega_R)$ . This happens while the line  $\mu_m^0(\Omega) = 0$  has a crossing too and the CR zone has already been created. The competition between the ILR and CR near their neighboring boundaries can therefore prohibit both resonances from broadening their zones and the disk develops a stationary wave. Right panel in Figure 7 shows the frequency space of the cored exponential disk together with the lines  $\mu_m^0(\Omega) = 0$  and  $\mu_m^{-1}(\Omega) = 0$  that have been drawn for  $\Omega_p = 0.1$  and  $m = 1, 2, 3$ . The line  $\mu_1^{-1}(\Omega) = 0$  never intersects the frequency space independent of the magnitude of  $\Omega_p > 0$ . A crossing is possible for  $m \geq 2$  and the slope of  $\mu_m^{-1}(\Omega) = 0$  increases proportional to  $m$ . Subsequently, the distance between the CR and ILR zones decreases by increasing  $m$  and the disk shows more reluctance against developing an unstable mode (see Figure 1 in Paper I). Bertin et al. (1977) had also reached a similar result for their three- and four-armed modes, and interpreted it based on the closeness of ILR and CR but with no mention of the increased likelihood of resonance overlapping.

Having resonant zones of finite width for both the CR and ILR is an essential prerequisite for their subsequent competition. The  $l$ th Fourier component in the radial angle can trap stars into a growing resonant zone if  $f_0(\mathbf{J})$  is smooth and non-zero on a range of manifolds of constant  $I_2 = J_R - lJ_\phi/m$ , and  $\mu_m^l(\Omega)$  can switch its sign in that neighborhood. Having some population of stars on circular orbits always guarantees the creation and growth of the CR zone because  $I_2$  is identical to  $J_R$  and  $I_1 = J_\phi/m$  can vary independently. However, if the ILR exists, its adiabatic invariant is defined by  $I_2 = J_R + J_\phi/m$  and the variation of  $I_1$  in the vicinity of a resonant value implies the variation of  $J_R$ . Therefore, the ILR can develop a growing resonant zone if  $f_0(\mathbf{J})$  has a functional dependence on both actions. Stellar disks with such a property will have non-zero radial velocity dispersions (warm disks).

Let me now consider a group of stars moving on near-

circular orbits that satisfy  $\mu_m^{-1}(\Omega) > 0$  and have been suddenly trapped into resonance by the ILR. On the resonant tori, the orbits of those stars are deformed so that  $I_2 = J_R + J_\phi/m$  remains constant. This means that orbits are elongated as  $J_R$  continuously increases from its tiny initial value and  $J_\phi$  drops until  $\mu_m^{-1}(\Omega)$  becomes negative and phase space flows reach their turning points. At this moment, some stars are likely to find themselves on the integral manifolds of constant  $J_R \gg 0$  and join the CR zone while they carry energy and angular momentum away from the ILR. A reverse migration is also possible. The switchings can only take place in the overlapping region of the ILR and CR where highly eccentric orbits live and  $\mu_m^{-1}(\Omega) < 0 < \mu_m^0(\Omega)$ . An effective early-stage overlap requires a non-zero  $f_0(\mathbf{J})$  in the cross section  $\mathcal{S}_m^0 \cap \mathcal{S}_m^{-1}$  of the sets

$$\mathcal{S}_m^0 = \{\Omega : \mu_m^0(\Omega) \approx \mathcal{O}(\epsilon)\}, \quad (88)$$

$$\mathcal{S}_m^{-1} = \{\Omega : \mu_m^{-1}(\Omega) \approx \mathcal{O}(\epsilon)\}. \quad (89)$$

As a result, infinitesimal wave amplitudes (in the linear regime) can suppress their own growth due to the competition between the CR and ILR. In the overlapping region  $\mathcal{S}_m^0 \cap \mathcal{S}_m^{-1}$  neither  $I_2 = J_R$  (for  $l = 0$ ) nor  $I_2 = J_R + J_\phi/m$  (for  $l = -1$ ) are conserved and that region is filled by chaotic orbits. The chaotic layer should be very narrow in the linear regime, but it will become thick in steady large-amplitude bars (Contopoulos 1983).

The stability of warm stellar disks for  $\Omega_p < \Omega_{\text{ILR}}(m)$  can be deduced from an independent mathematical reasoning as follows. Equation (74) applies to any growing resonant gap in the phase space. Let me assume that the ILR and CR of a wave with the pattern speed  $\Omega_p$  are widening their resonant zones with the rates

$$\dot{\Delta}_{\text{CR}}/\Delta_{\text{CR}} \sim s_1/2, \quad \dot{\Delta}_{\text{ILR}}/\Delta_{\text{ILR}} \sim s_2/2. \quad (90)$$

In an equilibrium disk with  $d\Sigma_0/dR < 0$ , the probability of capture into the ILR is more than the CR, and according to (90), we need  $s_2 > s_1$  to assure a faster expansion rate of the ILR zone. This inequality contradicts the basic assumption of linear analysis that separates the time-dependent part of perturbations as  $\exp(-\omega t)$  and assigns the same growing envelope and pattern speed to all parts of a normal mode. Therefore, the only possibility for a disk with a monotonic density gradient will be  $s_1 = s_2 = 0$ . In cold disks with  $f_0(\mathbf{J}) = \delta(J_R)g_0(J_\phi)$ , where  $\delta(J_R)$  is Dirac's delta function, the ILR cannot open a resonant gap because it suffers from the lack of

fuel (stars) needed for a possible expansion along the curves of constant  $I_2 = J_R + J_\phi/m$ . This automatically implies  $s_2 = 0$  and a unique value is assigned to  $s_1$ . The CR zone can thus grow freely and destabilize the disk.

It is worth noting that with an inner cutout, the surface density rises in central regions, reaches to a maximum and then decays outwards. Denote  $R_{\text{CR}}$  and  $R_{\text{ILR}}$  as the corotation and inner Lindblad radii, respectively. If the cutout is not sharp and the density peak lies fairly between  $R_{\text{ILR}}$  and  $R_{\text{CR}}$  (see the leftmost panel in Figure 8 of Evans & Read 1998b), it will be possible to find two points of the same density on the curve of  $\Sigma_0(R)$ : one near the ILR on the rising part of  $\Sigma_0(R)$  and the other near the CR on the falling side, i.e.,  $\Sigma_0(R_{\text{ILR}}) \approx \Sigma_0(R_{\text{CR}})$ . Thus, the ILR and CR can manage to grow with the same rate  $s_1 = s_2$  and an unstable mode emerges. Such modes have been demonstrated in Figure 7 of Evans & Read (1998b) whose cutout functions immobilize the circular orbits of the galactic center and all near-radial orbits. Accordingly, the population of active stars in the overlapping region of the ILR and CR declines substantially and the simultaneous growth of both resonances becomes likely. By decreasing the pattern speed, the ILR moves outside the cutout radius and its resonant zone becomes visible to the CR. The stellar disk is therefore stabilized. The condition  $s_1 = s_2 \neq 0$  cannot be reached if  $\Sigma_0(R_{\text{CR}})$  differs remarkably from  $\Sigma_0(R_{\text{ILR}})$ . This happens when both the ILR and CR lie outside the cutout radius or when the cutout is so sharp.

The above analysis shows how diverse the response of disk galaxies may be to non-axisymmetric excitations. Toomre (1981) suggested that the two parameters  $Q$  and  $X$  decide the fate of non-axisymmetric density waves. Wave mechanics based on the behavior of resonances, shows more complex decisive factors that govern the evolution of density waves, specially near the critical values of  $\Omega_p \approx \Omega_{\text{ILR}}(m)$  and for non-monotonic gradients of equilibrium density.

### 7.3. A Criterion for Global Stability

I am now in a position to provide a simple criterion for the stability of stellar disks in the absence of the ILR. It is the CR that captures stars, contributes an angular momentum imbalance to the stellar disk, and triggers unstable modes. Circumferential waves will be *globally stable* if resonant gaps do not open near the CR for all possible pattern speeds. Consequently,  $L_m(0)$  should remain zero, which according to equation (21) implies

$$\Lambda_{jk}^{m0} = 0, \quad \forall j, k \geq 0. \quad (91)$$

This condition is satisfied only if [see equations (16) and (17)]

$$\frac{\partial f_0}{\partial J_\phi} = 0, \quad \text{for all } \mathbf{J} \in \mathfrak{R}^+ \times \mathfrak{R}^+. \quad (92)$$

The stability criterion given in (92) can also be deduced from the earlier works of LBK and JH as I explain below. An alternative form of (20) is given in equation (B6) of JH as

$$\frac{d\mathcal{L}}{dt} = -2ms\pi^2 e^{2st} \sum_{l=-\infty}^{\infty} \int d\mathbf{J} \left( l \frac{\partial f_0}{\partial J_R} + m \frac{\partial f_0}{\partial J_\phi} \right)$$

$$\times \frac{|\tilde{V}_l|^2}{|l\Omega_R + m\Omega_\phi - \omega|^2}. \quad (93)$$

where

$$\tilde{V}_l = \sum_{j=0}^{\infty} \tilde{a}_j^m \tilde{\Psi}_j^{ml}(\mathbf{J}). \quad (94)$$

Dividing equation (93) by  $16\pi^4$  and changing the sign of  $\omega$  lead to equation (28) in LBK. The amount of angular momentum emitted/absorbed by the  $l = 0$  component is therefore determined by

$$\left[ \frac{d\mathcal{L}}{dt} \right]_{l=0} = -2(m\pi)^2 s e^{2st} \int d\mathbf{J} \frac{\partial f_0}{\partial J_\phi} \frac{|\tilde{V}_0|^2}{|m\Omega_\phi - \omega|^2}, \quad (95)$$

which reduces to equation (96) of Goldreich & Tremaine (1979) as  $s \rightarrow 0$ . It is seen that the sign of  $\partial f_0 / \partial J_\phi$  determines whether the angular momentum is added to, or drained from the  $l = 0$  wave component. Furthermore, the CR will not imbalance  $\mathcal{L}$  if the condition (92) holds. This means that the condition (84) cannot be violated according to my discussion of §6, and  $s$  should vanish for arbitrary perturbations. A stellar disk that satisfies (92) will be hot because it is impossible to reproduce the surface density gradient in the limit of  $J_R \rightarrow 0$  with a DF that does not depend on  $J_\phi$ . It has now become more transparent why there is a correlation between Toomre's (1964)  $Q$  and the disk stability for non-axisymmetric excitations. An illustrative example has been given in Figure 6 of Paper I. Most of S-modes disappear when the parameter  $N$  of the DF is decreased and more stars are distributed on near-radial orbits.

### 7.4. The Stability of Scale-Free Disks

Stability analysis of cuspy mass models has been a big puzzle in stellar dynamics since Zang (1976) computed the global modes of Mestel's (1963) disk and showed the importance of  $m = 1$  excitations. To tackle the singular center of Mestel's disk, he introduced an inner cutout that freezes central stars with diverging orbital frequencies. Evans & Read (1998a,b) followed the same procedure but for different cusp slopes. In spite of all these remarkable efforts, what H02 illustrated for the frequency space of scale-free potentials was indeed the key to resolve the long-standing stability problem of scale-free disks without any simplifying cutouts. The map of the angular sector that H02 plotted in his Figure 1 for the scale-free potentials (Touma & Tremaine 1997)

$$V_0(R) = \begin{cases} \text{sign}(\beta)R^\beta, & \beta \neq 0, \quad -1 < \beta < 2, \\ \ln R, & \beta = 0, \end{cases} \quad (96)$$

will be an angular sector in the  $(\Omega_R, \Omega_i)$ -space with the  $\Omega_R$ -axis and the straight line

$$\Omega_i = \left( \frac{1}{\sqrt{2+\beta}} - \frac{1}{2} \right) \Omega_R, \quad (97)$$

being its lower and upper boundaries, respectively. The slope of the upper boundary is always less than or equal to  $1/2$ . It is therefore obvious that except for  $m = 1$ , all  $\mu_m^{-1}(\Omega) = 0$  and  $\mu_m^0(\Omega) = 0$  lines will intersect the frequency space (whatever  $\Omega_p$  may be) and resonance overlapping between the CR and ILR can occur if there are

enough number of non-circular orbits. In other words, the radial velocity dispersion  $\tilde{\sigma}_u$  (defined in Evans & Read 1998a) should exceed a critical value  $\tilde{\sigma}_{u,\min}(m)$  to give rise to nonempty cross sections  $\mathcal{S}_m^0 \cap \mathcal{S}_m^{-1}$ . This is possible only for  $m > 1$  excitations and it suggests that scale-free disks are subject to  $m = 1$  instabilities. Finding  $\tilde{\sigma}_{u,\min}(m)$  is an open, yet conceivable, problem that can generalize Toomre's (1964) criterion to non-axisymmetric perturbations of scale-free disks. I explained in §7.2 that the ILR cannot help to stabilize cold disks. That argument applies to self-consistent scale-free disks as well, and strongly justifies the existence of  $\tilde{\sigma}_{u,\min}(m)$  for  $m > 1$ . Moreover, a stability condition like  $\tilde{\sigma}_u > \tilde{\sigma}_{u,\min}(m)$  may correlate with Lynden-Bell's (1993, equation 6-23) criterion, which has been formulated based on the angular dispersion of lobe tumble rates.

## 8. DISCUSSION AND CONCLUSIONS

I had already given an evidence in §5.3 that LBK's theory cannot be extended to large growth rates. Here I provide a more detailed analysis of LBK's mode mechanism. Taking the  $s \rightarrow 0$  limit of (93) leads to equation (30) of LBK. The resulting integrand of the  $l$ th component involves the term  $\delta(l\Omega_R + m\Omega_\phi - \omega)$  but its argument never becomes zero for  $l \leq -1$  as long as  $\Omega_p$  exceeds  $\Omega_{\text{ILR}}(m)$ . Once the delta function vanishes for  $\Omega_p > \Omega_{\text{ILR}}(m)$ , the angular momentum content of  $l \leq -1$  components remains zero. Therefore, angular momentum transfer between inner and outer resonances as suggested by LBK, is feasible only for  $\Omega_p < \Omega_{\text{ILR}}(m)$ . This is a constraint on the applicability of LBK's theory.

According to the arguments of §7.2 and the WKB theory, the ILR is not transparent to short wavelength disturbances with  $X \gg 1$  (Binney & Tremaine 2008; Mark 1974) and any developing spiral structure must be damped unless the ILR remains invisible to the CR. Therefore, an inconsistent point in LBK's paper is the imagination of an angular-momentum-transferring spiral structure while the condition  $\Omega_p < \Omega_{\text{ILR}}(m)$  has already abandoned the existence of such structures. An issue yet needs to be explained: If there is no spiral structure in stable disks, which mechanism does transfer the angular momentum between inner and outer resonances? In fact, in the limit of  $s \rightarrow 0$  the density components  $\Sigma_1^{l-}$  and  $\Sigma_1^{l+}$  become stationary waves that are azimuthally separated by a phase shift of  $90^\circ$  (like the components of mode B1 in Figure 2). Thus, they exert opposite gravitational torques on each other without any need for a communicating spiral structure.

In this paper I decomposed unstable modes of a model disk galaxy to its constituent Fourier components and showed how different components experience a gravitational torque. My results clearly showed that only the Fourier component associated with the CR generates a resonant zone in the phase space, and other components exchange angular momentum far from resonances. This result led me to introduce a new dynamical mechanism that triggers unstable modes. According to my calculations, an irreversible resonant capture of stars into the CR causes a synchronous precession of their orbital axes, which in turn, support a rotating density pattern. The emerged pattern grows because the resonant zone expands in the frequency space.

The irreversibility of resonant trapping is the most destructive event that happens in a stellar disk when a group of resonant stars with  $d_i < I_1 < d_o$  gain angular momentum forever. An immediate consequence of this phenomenon is the angular momentum imbalance in the disk, which requires proper reaction of other stars in order to conserve  $\mathcal{L}$ . This is how the Fourier components of  $l \neq 0$  are generated and the angular momentum transfer between them is initiated. Reacting stars do not have a librating  $\theta$  and they cooperate in a way that the quantity  $|\mu_m^0(\Omega)|$  remains small for all components.

Using the maps of resonance zones in the phase and frequency spaces, I argued that resonance overlapping should stop the growth of unstable modes and stabilize stellar disks in the presence of an ILR. I showed that for  $m > 1$  the emergence of an ILR is inevitable in scale-free models. The competition between the CR and ILR can therefore stabilize sufficiently warm scale-free disks against  $m > 1$  excitations. Evans & Read (1998b) suggested in §6.1 of their paper that self-consistent scale-free disks (without inner cutouts) do not admit growing non-axisymmetric modes at all, and they ruled out the possibility of a critical temperature. Their prediction is in agreement with my results except in two aspects: (i) Since the line  $\mu_1^{-1}(\Omega) = 0$  does not intersect the frequency space of scale-free models, there is no ILR to compete with a growing CR and density waves will be amplified for  $m = 1$ . (ii) The ILR in cold disks is very special and it cannot develop a resonant zone of finite size. It is therefore hard to believe a serious influence by the ILR on the phase space flows up to a critical temperature.

Note that each unstable mode dominates an isolated region of the frequency (action) space until a chaotic layer emerges due to resonance overlapping. The rate by which the chaotic layer diffuses itself in the phase space, is determined by the resistance of KAM tori against competing resonant zones. The limited space that the fastest growing bar mode occupies after its saturation (Khoperskov et al. 2007), is an  $N$ -body evidence for such a resistance of spiral modes that fill outer regions of the core exponential disk.

The other implication of resonance overlapping, which has observational support too, is that the central bar in grand-design barred spiral galaxies must join the spiral arms at the tips of the bar, which are the overlapping regions of two neighboring B and S modes in the frequency space (see Figure 7). I note that the pattern speeds of the spiral and bar components are not the same because these structures are associated with different modes. The overlapping region is filled by chaotic orbits that yield the turbulent mixing of density waves. This process can enhance star formation near the tips of the bar. If we accept this scenario, barred spiral galaxies should have been formed from hot stellar disks whose eigenfrequency spectra include few spiral modes. On the other hand, flocculent spirals with many wave packets will be the natural destiny of initially cold disks that give birth to a rich family of spiral modes.

The mathematical background for the nonlinear evolution of modes was developed in Paper I but that formulation is valid as long as averaging is allowed over angle variables. In the presence of chaotic orbits it is impos-

sible to average out resonant angles and some modifications are required to deal with the CBE in its full nonlinear form. I will present such modifications in Paper III with the aim of discovering the dynamical processes that generate different classes of barred and spiral structures.

I thank Scott Tremaine and Chris Hunter for their encouragement and stimulating discussions in the course

of my calculations and writing the manuscript. I also express my sincere thanks to the referee whose illuminating comments helped me to further my calculations and thoroughly revise the presentation and arguments of sections 5 through 8. The major part of this research was supported by the Institute for Advanced Study at Princeton, where I was an astrophysics visitor.

## REFERENCES

- Athanassoula, E. 2003, *MNRAS*, 341, 1179  
 Bertin, G., Lau, Y. Y., Lin, C. C., Mark J. W.-K., & Sugiyama, L. 1977, *Proc. Natl. Acad. Sci. USA*, 74, 4726  
 Binney, J., & Tremaine, S. 2008, *Galactic Dynamics* (Princeton: Princeton Univ. Press)  
 Byrd, G. G., & Howard, S. 1992, *AJ*, 103, 1089  
 Chirikov, B. V. 1979, *Phys. Rep.*, 52, 263  
 Contopoulos, G. 1983, *A&A*, 117, 89  
 Evans, N. W., & Read, J. C. A. 1998a, *MNRAS*, 300, 83  
 Evans, N. W., & Read, J. C. A. 1998b, *MNRAS*, 300, 106  
 Goldreich P., & Tremaine, S. 1979, *ApJ*, 233, 857  
 Hohl, F. 1971, *ApJ*, 168, 343  
 Hunter, C. 2002, in *Disks of Galaxies: Kinematics, Dynamics and Perturbations*, ASP Conference Proceedings, Vol. 275, ed E. Athanassoula, A. Bosma, & R. Mujica (San Francisco: Astronomical Society of the Pacific), 293 (H02)  
 Jalali M. A. 2007, *ApJ*, 669, 218 (Paper I)  
 Jalali M. A., & Hunter, C. 2005, *ApJ*, 630, 804 (JH)  
 Kalnajs, A. J. 1978, in *IAU Symp. 77, Structure and Properties of Nearby Galaxies*, ed. E. M. Berhuijsen & R. Wielebinski (Dordrecht: Reidel) 113  
 Khoperskov, A. V., Just, A., Korchagin, V. I., & Jalali, M. A. 2007, *A&A*, 473, 31  
 Lynden-Bell, D. 1993, in *Galactic Dynamics and N-Body Simulations*, editors Contopoulos, G., Spyrou, N. K., & Vlahos, L., Springer-Verlag, Berlin, 3  
 Lynden-Bell, D., & Kalnajs, A. J. 1972, *MNRAS*, 157, 1 (LBK)  
 Mark, J. W.-K. 1974, *ApJ*, 193, 539  
 Mathur, S. D. 1990, *MNRAS*, 243, 529  
 Mestel, L. 1963, *MNRAS*, 126, 553  
 Sellwood, J. A. 1981, *A&A*, 99, 362  
 Sellwood, J. A., & Kahn, F. D. 1991, *MNRAS*, 250, 278  
 Sellwood, J. A., & Binney, J. J. 2002, *MNRAS*, 336, 785  
 Toomre, A. 1964, *ApJ*, 139, 1217  
 Toomre, A. 1981, in *Structure and Evolution of Normal Galaxies*, ed S. M. Fall & D. Lynden-Bell (Cambridge: Cambridge Univ. Press), 111  
 Toomre, A. 1990, in *Dynamics and Interactions of Galaxies*, ed. Wielen, R., Springer-Verlag, Berlin, 292  
 Touna, J., & Tremaine, S. 1997, *MNRAS*, 292, 905  
 van Kampen, N. G. 1955, *Physica*, 31, 949  
 Winter, O.C., & Murray, C.D. 1997, *A&A*, 319, 290  
 Wisdom, J. 1980, *AJ*, 85, 1122  
 Zang, T. A. 1976, PhD Thesis, Massachusetts Institute of Technology, Cambridge, MA